Polymer Chemistry



PAPER View Article Online
View Journal | View Issue



Cite this: *Polym. Chem.*, 2019, **10**, 6037

UV-induced vesicle to micelle transition: a mechanistic study†

Craig A. Machado, D Roger Tran, Taylor A. Jenkins, D Amanda M. Pritzlaff, D Michael B. Sims, B Brent S. Sumerlin D and Daniel A. Savin D*

The morphology of self-assembled block copolymer aggregates is highly dependent on the relative volume fraction of the hydrophobic block. Thus, a dramatic change in the volume fraction of the hydrophobic block can elicit on-demand morphological transitions. Herein, a novel hydrophobic monomer containing a photolabile nitrobenzyl (Nb) protecting group was synthesized and incorporated into a block copolymer with poly(ethylene glycol) methacrylate. This motif allows for the hydrophobic volume fraction of the amphiphilic block copolymer to be dramatically reduced in situ to induce a morphological transition upon irradiation with UV light. Two amphiphilic block copolymers, Nb 94 and Nb 176, with hydrophobic weight fractions of 80% and 86%, respectively, were synthesized and their self-assembly in water studied. Nb 94 assembled into vesicles with R_h = 235 nm and underwent a morphological transition after 21 minutes of UV irradiation to spherical micelles with $R_h = 27$ nm, determined by dynamic light scattering and confirmed by transmission electron microscopy. At intermediate irradiation times (14-20 min), Nb 94 vesicles swelled to a larger size, but underwent a morphological transition over the course of hours or days, depending on the exact irradiation time. Nb 176 assembled into large compound vesicles with a hydrodynamic radius (R_h) of 973 nm, as determined by dynamic light scattering (DLS), which decreased to ca. 700 nm after 300 minutes of UV irradiation with no apparent morphological transition. This study elucidates the mechanism and kinetics of the morphological transitions of block copolymer assemblies induced by a change in the hydrophobic volume fraction of the polymer.

Received 20th August 2019, Accepted 21st October 2019 DOI: 10.1039/c9py01259a

rsc.li/polymers

Introduction

Polymeric self-assembly is governed by many different factors. The three major thermodynamic factors that determine morphology are (1) core chain stretching, (2) corona chain crowding, and (3) interfacial tension.^{1–3} One major factor which dictates morphology, that is easy to control synthetically, is the hydrophobic/hydrophilic balance of the block copolymer, wherein increasing hydrophobic content leads to a morphology progression from spherical micelles, to wormlike micelles, to vesicles.^{4,5}

In addition to static structures, it is possible to create self-assembled structures that respond to external stimuli. For example, pH can induce (dis)assembly of structures,⁶⁻⁸ swell structures and reduce the polymer chain density at the surface,⁹ and even induce morphology changes.^{10–12} Similar responses can be achieved with a thermal trigger by utilizing

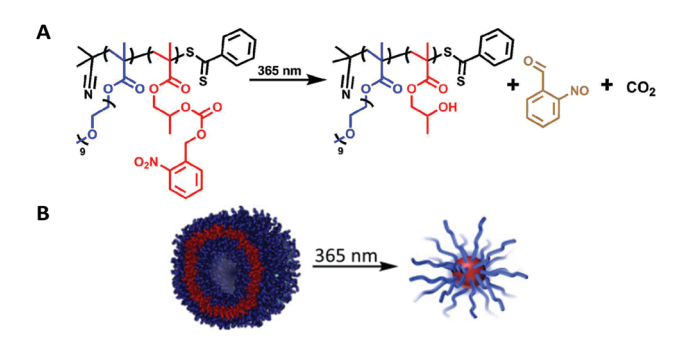
George & Josephine Butler Polymer Research Laboratory, Center for Macromolecular Science & Engineering, Department of Chemistry, University of Florida,

P.O. Box 117200, Gainesville, Florida 32611-7200, USA. E-mail: savin@chem.ufl.edu † Electronic supplementary information (ESI) available: Kinetic data, additional spectra, and supplemental plots and tables. See DOI: 10.1039/c9py01259a

Diels–Alder chemistry^{13,14} or the lower critical solution temperature (LCST) of certain polymers.^{15–20}

However, one stimulus that has received significant recent attention is light, largely due to the ability to apply irradiation with precise spatiotemporal control. Various molecular mechanisms of photo-responsiveness have been utilized, such as isomerization, 21,22 rearrangement, 23-25 crosslinking, 26-29 and cleavage. 30-33 For example, the irradiation of azobenzene with UV light results in isomerization from a hydrophobic trans conformation to a more hydrophilic cis isomer. Incorporation of this functionality into a block copolymer can allow for reversible micelle dissociation.³⁴ Reversibly core-crosslinked micelles can be achieved by incorporating pendant coumarin groups in the hydrophobic block of amphiphilic block copolymers, which can reversibly dimerize.35 Furthermore, the photocleavage of o-nitrobenzyl esters can be utilized to dissociate micelles by cleaving the junction point between the hydrophobic and hydrophilic blocks,36 depolymerizing the hydrophobic block,³⁷ or converting the amphiphilic block copolymer into a dual-hydrophilic block copolymer.38

Despite the variety of light-responsive micellar systems, very few reports of photocleavage-induced transition between selfassembled structures exist. Dong *et al.* synthesized light- and **Paper**



Scheme 1 Photolysis of block copolymer (A) and resulting vesicle to micelle transition (B).

poly(S-(o-nitrobenzyl)-L-cysteine-b-ethylene redox-responsive oxide), which assembled into vesicles.³⁹ Photocleavage of the nitrobenzyl group resulted in a morphology transition from vesicles to spherical micelles. However, to the best of our knowledge, there are no reports that investigate in detail the mechanism of the morphology changes due to changing the hydrophobic weight fraction in the block copolymer.

Herein, we report an amphiphilic block copolymer, which allows for a dramatic reduction in the hydrophobic weight fraction and associated morphology transition upon exposure to UV light. A novel monomer, nitrobenzyl hydroxypropyl methacrylate (NbHPMA), was synthesized to afford photo-responsiveness within the hydrophobic block. The resultant polymer self-assembles into vesicles and can undergo a morphological transition to spherical micelles with UV irradiation, as shown in Scheme 1. Dynamic light scattering (DLS) was used to characterize the solution self-assembly and morphological transition while transmission electron microscopy (TEM) confirmed the morphology. This study monitors the assemblies throughout various stages of the process, providing key insight into the kinetics and mechanism of the morphological transition.

Experimental

Materials and methods

Tetrahydrofuran (THF), dichloromethane (DCM), and dimethyl formamide (DMF) were purchased from Fisher. Phosgene (15 wt% in toluene), 2,2'-azobis(2-methylpropionitrile) (AIBN), 4,4'-azobis(4-cyanovaleric acid), potassium ferricyanide, benzyl chloride, sodium methoxide (30 wt% in methanol), and poly (ethylene glycol) methacrylate (PEGMA) were purchased from Aldrich. Hydroxypropyl methacrylate (HPMA, mixture of isomers), 4-dimethylamino pyridine (DMAP), and 1,4-dioxane were purchased from Acros. Hexanes, ethyl acetate, methanol, and silica gel were purchased from VWR. 2-Nitrobenzyl alcohol and sodium methoxide were purchased from Alfa Aesar, 2,2'azobis(4-methoxy-2,4-dimethylvaleronitrile) (V-70) was purchased from Wako Chemical, sulfur was purchased from Santa Cruz Biotechnology, and deuterated chloroform was purchased from Cambridge Isotope Laboratories. PEGMA and 1,4dioxane were passed through a plug of basic alumina prior to polymerization and 4,4'-azobis(4-cyanovaleric acid) was dried under vacuum overnight prior to use. All other materials were used as received.

TEM

Transmission electron microscopy was conducted using an H-7000 from Hitachi High Technologies America, Inc., Schaumber, IL USA. Digital images were acquired with a Veleta 2k × 2k camera and iTEM software (Olympus Soft-Imaging Solutions Corp., Lakewood, CO). Electron microscopy sciences carbon film on 300 square mesh copper grids (CF300-Cu) or silicon monoxide substrates on 300 mesh copper grids (SF300-Cu) were used for all measurements. Grids were glow discharged prior to sample preparation. A 10 µL droplet of polymer solution was placed on a parafilm square, and the grid was placed on top of the droplet. The grid was allowed to rest on top of the droplet for 1 minute before removing and wicking the excess solvent with filter paper. The grid was air dried overnight.

Dynamic light scattering

Multi-angle dynamic light scattering (DLS) analysis was performed on an ALV/CGS-3 four-angle, compact goniometer system (Langen, Germany), which consisted of a 22 mW HeNe linear polarized laser operating at a wavelength of λ = 632.8 nm and scattering angles from $\theta = 30-150^{\circ}$.

For DLS, fluctuations in the scattering intensity were measured via an ALV/LSE-5004 multiple tau digital correlator and analyzed *via* the intensity autocorrelation function $(g^{(2)}(\tau))$. Decay rates, Γ , were obtained from single-exponential fits using a second-order cumulant analysis, and the mutual diffusion coefficient, $D_{\rm m}$, was calculated through the relation

$$\Gamma = q^2 D_{\rm m}$$

where q^2 is the square of the scalar magnitude of the scattering vector. The hydrodynamic radius (Rh) was then calculated through the Stokes-Einstein equation

$$D_{\rm m} \approx D_0 = \frac{k_{\rm B}T}{6\pi\eta_{\rm s}R_{\rm h}}$$

where $D_{\rm m}$ is approximately equal to the self-diffusion coefficient (D_0) , k_B is the Boltzmann constant, T is the absolute temperature, and η_s is the solvent viscosity.

Gel permeation chromatography

Absolute molecular weights and molecular weight distributions of polymers were obtained via multi-angle laser light scattering size-exclusion chromatography (MALS-SEC) and calculated using Wyatt ASTRA software. N,N-Dimethylacetamide (DMAc) with 50 mM LiCl was used as a solvent at 50 °C and a flow rate of 1 mL min⁻¹ was used (Agilent isocratic pump, degasser, and autosampler; ViscoGel I-series 10 µm guard column and two ViscoGel I-series G3078 mixed bed columns, with molecular weight ranges $0-20 \times 10^3$ and $0-10 \times 10^6$ g mol^{-1} , respectively).

Nuclear magnetic resonance

¹H and ¹³C NMR spectroscopies were performed on an Inova 500 MHz, 2 RF channel instrument or Mercury 300 MHz 4-nuc instrument at 25 °C. Samples were dissolved in CDCl₃.

Synthesis and experimental procedures

Synthesis of 2-nitrobenzyl chloroformate (NbC). A 100 mL Schlenk tube was charged with a stir bar, phosgene (15 wt% in toluene, 30.0 mL, 41.4 mmol) and dry THF (5 mL). 2-Nitrobenzyl alcohol (2.57 g, 16.8 mmol) was dissolved in THF (15 mL) and added to the reaction mixture dropwise. The flask was wrapped in aluminum foil and stirred at room temperature for two days. Then, argon was bubbled through the solution to remove dissolved phosgene and the exhaust was bubbled through a solution of sodium carbonate and sodium hydroxide. Solvent was removed under vacuum to afford NbC as a brown oil. Note: Solvent was removed on a Schlenk line rather than rotary evaporator to ensure excess phosgene was contained in solvent trap and not exhausted into the laboratory. Conversion was determined via thin layer chromatography (TLC), and NbC was used immediately in the next

Synthesis of nitrobenzyl hydroxypropyl methacrylate (2-((((2nitrobenzyl)oxy)carbonyl)oxy)propyl methacrylate, (NbHPMA)). To a 100 mL round bottom flask with stir bar was added HPMA (3.1 g, 21.5 mmol), DMAP (4.01 g, 33.5 mmol), and dry CH₂Cl₂ (10 mL), and the mixture was stirred on ice. NbC (3.6 g, 17 mmol) was dissolved in dry CH₂Cl₂ (15 mL) and added to the solution dropwise. The flask was then wrapped in aluminum foil and stirred at room temperature. Reaction progress was monitored by TLC, and upon full conversion, the solution was washed three times with 5% aqueous HCl to remove DMAP salts, and the solvent was removed by vacuum. The crude product was purified by flash chromatography in CH_2Cl_2 , with an R_f value of 0.4, to afford a yellow oil (4.28 g, 79% yield).

Synthesis of 4-cyano-4-(phenylcarbonothioylthio) pentanoic acid (CPDB). CPDB was synthesized according to a procedure adapted from McCormick, et al.40 To a flame-dried 100 mL bottom flask equipped with magnetic stir bar was added 30 wt% sodium methoxide in methanol (12.7 g, 70.4 mmol). The flask was purged with argon, then anhydrous methanol (20 mL) was added via cannula followed by the addition of elemental sulfur (2.25 g, 70.4 mmol) under positive argon flow. The flask was sealed with a rubber septum, then benzyl chloride (4.46 g, 35.2 mmol) was added dropwise over 10 min. The suspension was then heated to 65 °C and stirred for 8 h. After this, the resultant dark red solution was cooled to 0 °C, filtered, and evaporated to a residue. DI H2O (30 mL) was added, followed by a second filtration. The filtrate was transferred to a separatory funnel, washed with diethyl ether (15 mL), then acidified with 1.0 N HCl solution (30 mL). This was then extracted with diethyl ether (3 × 15 mL) to produce an ethereal solution of dithiobenzoic acid, which was then back-extracted with 0.66 N NaOH solution (3 × 60 mL) to yield an aqueous solution of sodium dithiobenzoate.

Next, this solution was transferred to a 500 mL Erlenmeyer flask equipped with magnetic stir bar. Under vigorous stirring, a solution of potassium ferricyanide (11.6 g, 35.2 mmol, 1.0 equiv.) in DI H₂O (175 mL) was added dropwise over 1 h. The resultant precipitate was filtered, washed with excess DI H2O, and dried in vacuo to yield bis(thiobenzoyl) disulfide as a red

The disulfide (2.33 g, 7.60 mmol) was combined with 4,4'azobis(4-cyanovaleric acid) (3.20 g, 11.4 mmol) in a 2-neck round bottom flask equipped with reflux condenser, taken up in ethyl acetate (40 mL), sealed, and purged with argon for 1 h. After purging, the reaction was heated to 70 °C and stirred at reflux for 18 h. The red solution was then evaporated and the crude product purified by flash chromatography (1% acetic acid in 3/2 hexanes/ethyl acetate). The combined fractions corresponding to product were reduced to a volume of \sim 50 mL, washed with brine (3 × 25 mL) to remove acetic acid, then dried over sodium sulfate and filtered. This solution was reduced to a residue then recrystallized from hot benzene to yield 4-cyano-4-(phenylcarbonothioylthio) pentanoic acid as a pink solid (2.09 g, 21% yield).

Synthesis of poly(PEGMA) macro-chain transfer agent (CTA). A stock solution of AIBN (11.5 µg, 70.0 µmol) in THF was added to a 25 mL Schlenk tube with a magnetic stir bar. THF was removed and CPDB (100 mg, 0.360 mmol), PEGMA (3.50 g, 7.00 mmol), and 1,4-dioxane (4.1 mL) were added to the flask and stirred until dissolved. The solution was degassed via three freeze-pump-thaw cycles, then the flask was stirred at 70 °C. After 140 min, the solution was removed from heat and exposed to air to terminate polymerization. The reaction mixture was dialyzed against deionized water and polymer was isolated by lyophilization (1.04 g, 38% yield).

Synthesis of polymers Nb 94 and Nb 176. Nb 94 was synthesized as follows: to a 25 mL Schlenk tube with a magnetic stir bar were added poly(PEGMA) macro-CTA (0.203 g, 0.0270 mmol), 1,4-dioxane (0.90 mL), and NbHPMA (1.38 g, 4.26 mmol). The tube was covered with aluminum foil and the solution was purged on ice for 20 min. In a separate vial, a stock solution of V-70 (8.3 mg, 0.027 mmol) was prepared in cold, purged DMF (1 mL). An aliquot (0.20 mL, 0.0054 mmol V-70) of this initiator solution was added to the Schlenk flask and the flask was purged on ice. After 15 min, the flask was immersed in a water bath and stirred at 35 °C. Kinetic aliquots (50 µL) were taken periodically with a purged syringe, and when the conversion reached ca. 50%, the polymerization was stopped by exposure to air and precipitation into diethyl ether. Polymer was collected by centrifugation and dried in vacuo (0.67 g, 72%). The same procedure was used to synthesize Nb 176, but with a monomer to poly(PEGMA) molar ratio of 250:1.

Self-assembly of polymers

A 2 mL vial was loaded with Nb 94 or Nb 176 (20 mg) and 1 mL of dimethyl formamide (DMF), and the mixture was stirred until dissolved. Ultrapure water (1 mL, equal to volume of DMF) was added at a rate of 18 µL per minute (1.8 vol% per

min) *via* syringe pump with stirring. The resulting milky white solution was dialyzed against ultrapure water for 2 days with 8 water changes to afford an aqueous polymer solution with a concentration of 0.50 wt%.

Preparation of light scattering samples

Light scattering cuvettes (10 mm borosilicate glass) were cleaned by inverting the cuvette and rinsing with 10 mL of ultrapure water and shaking off excess water. To the cleaned cuvette, 0.90 mL of ultrapure water was added along with 50 μL of polymer vesicle solution. The cuvette was capped, and the solution was vortexed to thoroughly mix, resulting in a final polymer concentration of 0.025 wt%. Solutions were scattered without additional filtering, so as not to alter the large assemblies.

Photolysis

Light scattering cuvettes were irradiated in a U-Spicy USND-3601 UV curing apparatus. Samples were irradiated for a given amount of time with a strong air flow blowing on cuvette to prevent overheating. Immediately after irradiation, samples were analyzed by light scattering.

Results and discussion

Synthesis of monomer and polymers

In order to achieve a morphology transition based on changing the volume fraction of the hydrophobic block, the block must be hydrophobic before and after photo-cleavage. However, if the block is too hydrophobic, the assembly may remain kinetically trapped in the initially-prepared state and be unable to rearrange into a more favorable morphology. Therefore, poly (HPMA) was chosen for the hydrophobic block as it is insoluble in water, yet is still relatively polar, which will allow for some minimal hydration. Additionally, the hydroxyl moiety provides a convenient handle for attaching the nitrobenzyl protecting group. Scheme 2 shows the synthetic pathway towards nitrobenzyl HPMA (NbHPMA).

Briefly, nitrobenzyl alcohol was added to a solution of phosgene to produce nitrobenzyl chloroformate (NbC). Synthesis of NbC was confirmed by ¹H and ¹³C NMR spectroscopy, as shown in Fig. S1 and S2.† Crude NbC was immediately reacted with HPMA and DMAP, and NbHPMA was purified by column chromatography. Synthesis and purity of NbHPMA were con-

Scheme 2 Synthetic scheme for NbHPMA.

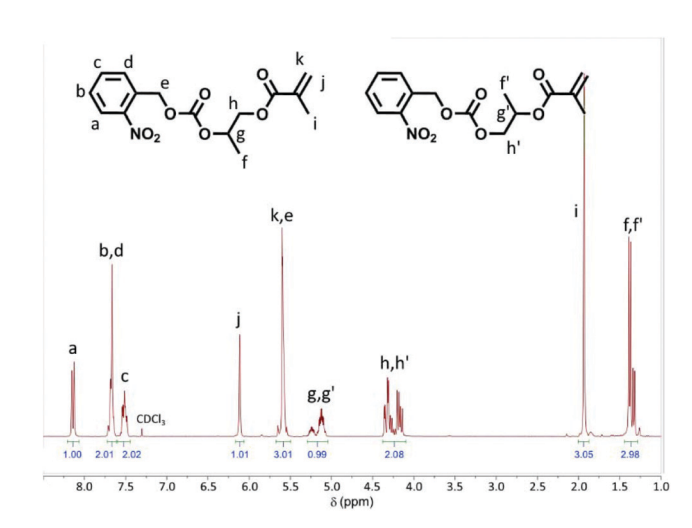


Fig. 1 $\,^{1}$ H NMR spectrum of NbHPMA. Note: HPMA was purchased as a mixture of isomers.

firmed by ¹H (Fig. 1) and ¹³C NMR spectroscopy (Fig. S3†) as well as high resolution mass spectrometry (HRMS) and liquid chromatography-mass spectrometry (LC-MS) (Fig. S4–S8†).

Next, poly(PEGMA) macro-chain transfer agent (macro-CTA) was synthesized and was characterized by gel permeation chromatography (GPC, Fig. 2) and ¹H NMR (Fig. S9†). The polymerization was well-controlled, with a symmetric trace, a *D* of 1.04, and a degree of polymerization (DP) of 18 determined *via* light scattering detection (Fig. 2, red trace).

Having synthesized NbHPMA and macro-CTA, a block polymerization was attempted, targeting a DP of 55 for the NbHPMA block. However, polymerization did not follow a pseudo-first order kinetic plot (Fig. S10†), yet an acceptable dispersity of ~1.2 was achieved. To better understand the kinetics of poly(NbHPMA) polymerization, a homopolymerization was carried out with the CPDB CTA at 70 °C with AIBN as a radical initiator. As found above, this control reaction did not strictly obey pseudo-first order kinetics. Molecular weight distributions exhibited both low-molecular-weight tailing and high-molecular-weight shouldering, and dispersity increased slightly with increasing polymerization time (Fig. S14 and S15†).

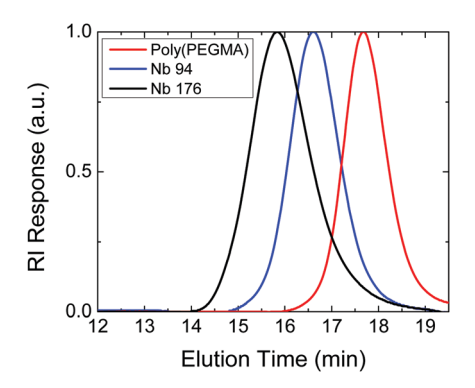


Fig. 2 Symmetric GPC traces of Nb 94 (blue), Nb 176 (black) and poly (PEGMA) macro-CTA (red) showing well-controlled polymerization.

Table 1 Physical characteristics of block copolymers

Polymer	PEGMA DP	NbHPMA DP	$M_{\rm n}~({ m g~mol^{-1}})$	Đ	% hydrophobic before photolysis	% hydrophobic after photolysis (theoretical)
Nb 94	15	94	37 900	1.10	80	64
Nb 176	18	176	65 800	1.09	86	74

These observations are consistent with side reactions commonly observed during the polymerization of o-nitrobenzylcontaining monomers, 43 involving either inhibitory chain transfer to the nitrophenyl ring (low molecular weight tails) or transfer to the benzyl methylene group that produces branched polymers (high molecular weight shoulders). Therefore, to reduce these unwanted side reactions, polymerizations were conducted at reduced temperature (35 °C) using a low-temperature radical initiator, V-70. At this lower temperature, good control was observed, as evidenced by symmetric GPC traces uniformly shifting to lower elution times and linear pseudo-first order kinetic and M_n vs. conversion plots (Fig. S16-S18†). However, D increased with increasing conversion, therefore we decided to run future polymerizations to low (<40%) conversion. Physical characteristics of the polymers studied are listed in Table 1.

Self-assembly of polymers

After synthesizing the block copolymers, we intended to induce self-assembly into vesicles in aqueous solution. Polymers Nb 94 and Nb 176 were individually dissolved in THF, a good solvent for both blocks, and multiple methods were used to induce assembly. First, nanoprecipitation was attempted by adding water at a rate of 1 mL h⁻¹, followed by evaporation of THF under ambient conditions. Despite varying the initial concentrations and ratios of water to THF, only small micelles were obtained for both polymers, with hydrodynamic radii of 15 nm for Nb 94 and 24 nm for Nb 176 (Tables S1 and S2†). Next, solutions of polymers in THF were dialyzed against water. Polymers were dissolved at 1-5 mg mL⁻¹ in THF, then dialyzed against THF/water mixtures, with each change of dialysate increasing in water content before dialyzing against pure water. Again, however, only small micelles were obtained for both polymers, with hydrodynamic radii of 13 nm for Nb 94 and 34 nm for Nb 176. Thin film hydration was attempted as well, however the polymer showed insufficient solubility in pure water.

Inspired by an Eisenberg study that details the effect of organic solvent choice on morphology of the self-assembled structure, ⁴⁴ we decided to explore other solvents. Dioxane was investigated first, and 10 mg of Nb 176 were dissolved in 0.5 mL of dioxane, and 0.5 mL of water was added at a rate of 9 μ L min⁻¹, and then the solution was dialyzed against water. The resulting solution had a concentration of 0.46 wt% and was strongly opalescent. However, the R_h was 28 nm, similar to previous attempts at vesicle synthesis.

The same procedure was used with DMF, and a milky white suspension was obtained after addition of water and persisted

through dialysis. This suspension appeared colloidally stable, but showed some settling over the course of several hours. As this solution was too opaque to run DLS, suspensions were diluted 20-fold in water for DLS analysis. DLS showed an $R_{\rm h}$ of 973 nm, which would be consistent with vesicle formation. This procedure was applied to Nb 94 and similar results were observed, with an $R_{\rm h}$ of 438 nm. Therefore, we proceeded with this self-assembly procedure for all experiments discussed below.

Photolysis on block copolymers

To test the evolution of assembly size as a function of irradiation time, a light scattering cuvette containing polymeric assemblies was placed in a U-Spicy UV curing lamp for a given amount of time, then analyzed by DLS. A single cuvette of Nb 94 or Nb 176 assemblies was subjected to cycles of irradiation and light scattering analysis to construct Fig. 3 and 9, respectively.

Up to 25 minutes of irradiation on Nb 94 assemblies resulted in a slight increase in radius, from 438 to 512 nm. However, the next day (with no further irradiation), large particulates were not visible, and the solution was clear with a brown color (see Fig. 5). DLS showed that the particles decreased from 512 nm to 72 nm overnight despite the solution not being subjected to further irradiation (red open box in Fig. 3). We believe the assemblies here undergo a morphology transition from vesicles to spherical micelles, but the transition is a slow process. Further irradiation (35 min) caused the radius to decrease to 38 nm.

With the knowledge that there is a time-dependence to the photo-responsive behavior, a slight change in procedure was necessary. Rather than conducting the entire photolysis experiment on one sample (as was done for Fig. 3 and 9), a new,

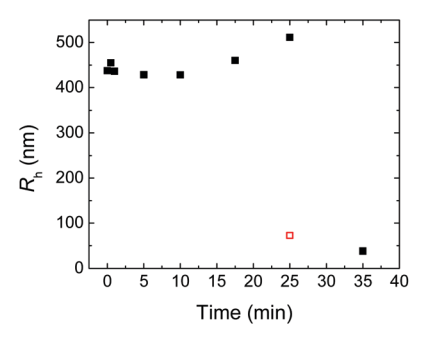


Fig. 3 R_h of Nb 94 assemblies as a function of UV-irradiation time. Red open box indicates solution measured after \sim 19 h with no further irradiation.

Paper

300 250 200 200 150 1 II III 50 0 10 20 30 100 Time (min)

Fig. 4 Second trial determining $R_{\rm h}$ of Nb 94 assemblies as a function of UV irradiation time showing regimes I (blue), II (yellow), and III (green). Black squares indicate $R_{\rm h}$ immediately after irradiation and red open boxes indicates the same solution measured after ~19 h with no further irradiation. Note: Radii were unchanged for samples irradiated for 10 min or less. Scattering intensity was too low to obtain next-day data for 32 and 100 min solutions.

larger-scale solution of assemblies was prepared, and a new cuvette was prepared for each time point for Fig. 4 to investigate how aggregate sizes changed over time with the given irradiation time. Fig. 4 shows R_h as a function of irradiation time, with black squares representing R_h immediately after irradiation and open red squares representing R_h of the same solution measured the next day with no additional irradiation. This new solution contained particles with an initial R_h of 235 nm. Upon irradiation, the same qualitative behavior was observed which can be divided into three distinct regimes: an initial decrease in size (to 182 nm), swelling at intermediate irradiation times (up to 273 nm), followed by a morphology transition (at 21 minutes, with assembly size decreasing to 27 nm).

In regime I, when samples were irradiated between 0 and 10 min, there was a small decrease in assembly size. This is consistent with small decreases in the hydrophobic fraction, but no significant morphology changes. When samples were irradiated between 12 and 22 min (regime II), there is a pronounced increase in assembly size initially, indicated by the black data points. However, the red squares show two subregions of photoresponse and associated morphology changes. First, when samples were irradiated between 12 and 16 minutes and allowed to sit in the dark, assemblies swelled initially and remained swollen overnight, leading to an increased R_h the next day. However, for samples irradiated for 18-21 min, the assemblies initially swelled (black points), but then appeared to undergo a morphology transition while sitting overnight (red points), decreasing from ca. 273 to 75 nm at 18 min irradiation. Once assemblies were irradiated for over 21 min (regime III), the morphology transition occurred immediately, with only a slight decrease in radius the next day. Fig. 5 shows the visual clarity of solutions after 0 and 22 min of irradiation. Note the haziness of the solution prior to irradiation, indicating the presence of larger assemblies. After the morphological transition, the solution is clear, with only a brown tint from the nitrosobenzaldehyde byproduct.



Fig. 5 Photos of Nb 94 assemblies from Fig. 4 after 0 and 22 min of irradiation.

We decided to further investigate the time-dependent morphology transition of Nb 94 assemblies by monitoring intensity of scattered light as a function of time. A fresh solution of Nb 94 vesicles was irradiated for 18 min, DLS was performed to determine $R_{\rm h}$, and then the scattering intensity was measured as a function of time. Fig. 6 shows a large drop-off in intensity within the first 5 h, followed by a gradual decrease in intensity for the duration of the experiment. The excess scattered intensity is dependent on molecular weight of the scattering species and can be approximated by the equation

$$R_{\theta} = KcM(1 - 2BcM)P(\theta)$$

where R_{θ} is the normalized excess scattered intensity per unit volume, c is concentration, M is the molecular weight of the scattering body (*i.e.*, assemblies), K is an optical constant, B is the second osmotic virial coefficient, and $P(\theta)$ is the form factor. While Fig. 6 does not show excess scattered intensity, the scattering from solvent was low enough (<1%) such that the excess intensity was approximately equal to the total intensity. From this equation, a decrease in scattered light intensity corresponds to a decrease in molecular weight (*i.e.*, aggregation number) of the assemblies, with the size ($R_{\rm h}$) of the assemblies gradually decreasing with time with as shown in Fig. 6; this result is consistent with the morphology transition being a gradual process rather than an instantaneous one. It is also possible to have changes in excess scattering that result from dramatic changes in the form factor or osmotic virial

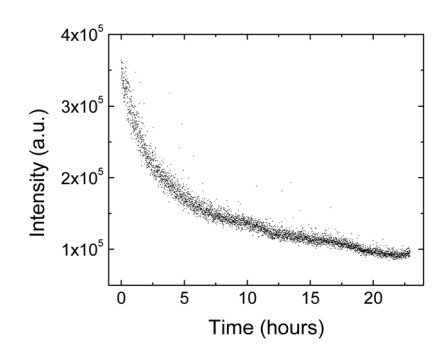


Fig. 6 Scattered intensity of Nb 94 solution as a function of time after 18 min of UV-irradiation.

Polymer Chemistry

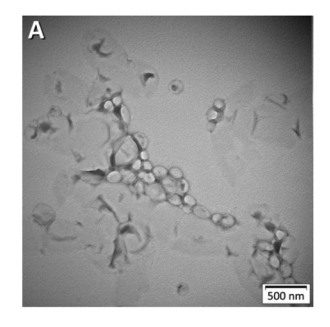
coefficient. For the former effect, in general the scattered intensity decreases with increasing assembly size (and angle), in contrast to what is observed in the R_h data for this transition. For the latter effect, in general the osmotic effects on scattering are dominated by the corona block, unless there is a critical point that leads to a unimer-micelle type of transition. In the case of Nb assemblies, the thermodynamics associated with the corona block remain largely unchanged.

After characterizing the kinetics of the overnight transition, we hypothesized that the morphological transition could be accelerated with the input of additional energy. A solution was irradiated for 18 min, followed by sonication for 10 min. DLS showed an Rh of 65 nm, indicating that sonication provided sufficient energy to induce an immediate morphology transition, despite the transition occurring over the course of ~20 hours without sonication. After sonicating the same solution for an additional 10 min (20 min total), the R_h was 54 nm, showing a further size evolution with additional energy input. These experiments display another mechanism of control over the kinetics of the morphology transition.

To further explore the mechanism of the morphology transition, we elected to employ depolarized light scattering to probe the presence of anisotropic intermediates. Vesicle formation often occurs through fusion of spherical micelles into wormlike micelles, fusion of wormlike micelles into branched intermediates (such as jellyfish and octopi), followed by coalescence of the branches into a sheet, and curvature into a spherical vesicle.^{5,46} If the vesicle-to-spherical micelle transition occurred through the reverse of this process, then depolarized light scattering should detect elongated structures such as wormlike micelles, whereas isotropic particles such as vesicles and spherical micelles should produce low scattering intensity in a depolarized experiment. 47 Fig. S25† shows that low scattering intensity is observed throughout the course of the experiment, with a gradual monotonic decrease in intensity with time. If an elongated intermediate was observed during the morphological transition, depolarized scattering intensity would be expected to increase. However, the same trend was observed as that in Fig. 6, suggesting that the morphological transition does not proceed through an elongated intermediate.

TEM

To confirm the morphology of self-assembled structures, solutions were analyzed by transmission electron microscopy (TEM). ImageJ was used to calculate the radii of structures. Prior to irradiation (Fig. 7A), TEM images of Nb 94 assemblies show vesicles with an average radius of 56 nm. However, some of the larger vesicles measured up to 214 nm in radius. These numbers are consistent with a measured Rh of 235 nm from DLS, as DLS tends to bias larger particles in the reported average. The broad size distribution of particles observed in Fig. 7A is in agreement with DLS, which shows a PDI (normalized second cumulant) of ~0.4. After 100 min of irradiation (Fig. 7B), TEM confirms the morphological transition to spherical micelles. The micelles appear somewhat polydis-



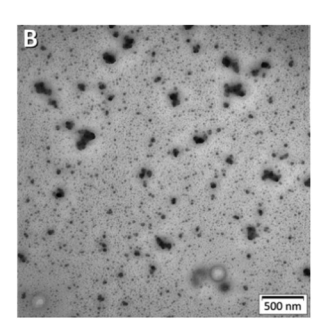


Fig. 7 TEM micrographs (unstained) of Nb 94 assemblies at 0 min (A) and 100 (B) min of UV-irradiation.

perse, with some large and some small micelles with radii of 28 and 9 nm, respectively. Again, the broad dispersity and size values are consistent with DLS, which shows a PDI and R_h of ~0.5 and 28 nm, respectively. Fig. S26 and S27† show representative CONTIN plots (for 0 and 100 min irradiation, respectively) which show broad, but unimodal distributions.

To view the intermediate, swollen structures, a sample was irradiated for 16 min, then cast on a TEM grid. As shown in Fig. 8, ill-defined aggregates were observed at intermediate irradiation times. An average radius of 260 nm was measured, which agrees well with the Rh of 251 nm measured by DLS. Interestingly, the transient assemblies appear somewhat clover-shaped. There is precedent⁴⁸ for the vesicle-to-micelle transition undergoing the reverse of the micelle-to-vesicle transition observed by Armes and coworkers, proceeding through jellyfish and octopi intermediates. However, our system appears to involve a different mechanism, with spherical micelles apparently "budding" off of ill-defined sheet-like aggregates. Several of these "buds" were measured and were found to have an average radius of 120 nm, which is somewhat larger than the largest Rh measured after assemblies underwent the morphological transition (75 nm, the day after irradiating for 18 min), further supporting the proposed budding mechanism. However, the nature of this budding is not known at this time. One possible explanation is that a decrease in hydrophobic volume results in an increase in interfacial curvature. This may result in instabilities at the interface that create these buds of higher curvature. This explanation is qualitat-

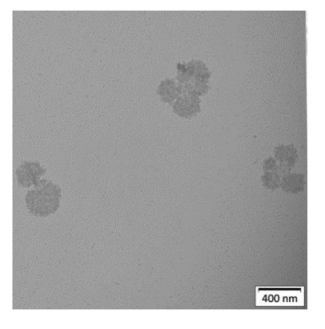


Fig. 8 TEM micrograph of transitional Nb 94 structures after 16 min of

ively consistent with the kinetics of this transition as well. As the irradiation time increases, there is a production of nitrosobenzaldehyde in the membrane of the vesicles that can cause initial swelling. As the nitrosobenzaldehyde diffuses from the membrane, the interfacial changes can occur. A direct transition from vesicles to budding structures to micelles is also consistent with the absence of elongated transient structures during the transition.

Comparison of NB 94 and Nb 176

Next, photolysis was conducted on Nb 176 assemblies, and the $R_{\rm h}$ are plotted as a function of irradiation time in Fig. 9. Fig. 9 shows a decrease in radius from ca. 1000 to 650 nm after 420 min of irradiation. Prior photolysis experiments on assemblies showed that at 420 min of irradiation, 94% of nitrobenzyl groups were cleaved as monitored by $^{1}{\rm H}$ NMR (Fig. S28†), suggesting further irradiation will likely not induce any more changes. Based on the modest decrease in $R_{\rm h}$, we propose that the assemblies decreased in size from the cleavage of nitrobenzyl side chains but did not undergo a morphology transition, in contrast to Nb 94 assemblies.

To investigate whether the lack of morphology change was due to the assemblies being kinetically trapped or whether the final assemblies are the preferred structure and size, two control experiments were performed. First, a block copolymer, poly(PEGMA₁₈-b-HPMA₁₇₈), with the same DPs as Nb 176 - but no nitrobenzyl group - was synthesized and assembled under identical conditions to simulate Nb 176 after 100% photolysis of nitrobenzyl groups. Given that ~94% of the nitrobenzyl groups have been cleaved at 420 min irradiation, we believe poly(PEGMA₁₈-b-HPMA₁₇₈) should provide an adequate comparison to the self-assembly behavior of Nb 176 after photocleavage. If the photolyzed Nb 176 assemblies represented thermodynamically favorable structures, this poly(PEGMA₁₈-b-HPMA₁₇₈) should assemble into structures in the 600-800 nm range. If, however, the assemblies were significantly smaller, then the photolyzed Nb 176 assemblies likely remain kinetically trapped at their large size. DLS on poly(PEGMA18-b-HPMA₁₇₈) assemblies showed an R_h of 28 nm, suggesting that the Nb 176 assemblies may be kinetically trapped because they did not rearrange to similarly-sized micelles. However, this study does not account for the small amount of remaining nitrobenzyl groups on Nb 176 nor the released nitrosobenzal-

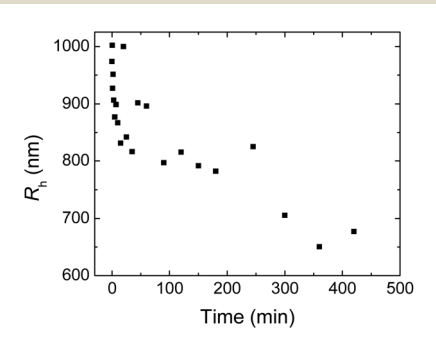
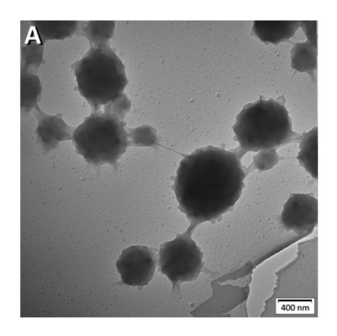


Fig. 9 R_h of Nb 176 assemblies as a function of UV-irradiation time.



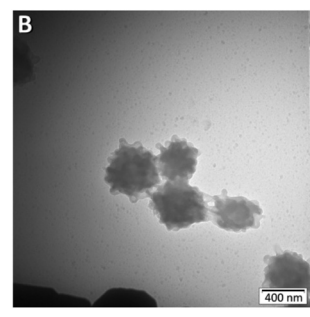


Fig. 10 TEM micrographs of Nb 176 assemblies at 0 (A) and 100 (B) min of UV-irradiation.

dehyde. Therefore, another control experiment was designed which would account for these factors. Nb 176 was dissolved in THF and irradiated for 100 minutes. THF was removed, Nb 176 was redissolved in DMF, and Nb 176 was assembled as described previously. After dialysis, assemblies were found to have an $R_{\rm h}$ of 1010 nm. Additionally, the solution remained brown after dialysis, indicating that much of the nitrosobenzaldehyde remained trapped within the hydrophobic core rather than diffusing out. These results suggest that nitrosobenzaldehyde trapped within the hydrophobic membrane of the vesicle after photo-cleavage prevents Nb 176 assemblies from rearranging into spherical micelles.

Finally, assemblies of Nb 176 were imaged and found to have an average radius of 464 nm compared to an $R_{\rm h}$ of 519 nm measured by DLS prior to irradiation. Fig. 10A shows that the Nb 176 assemblies do not appear to be vesicular in morphology, due to the dark centers and irregular surface. However, the structures may be large compound vesicles, as evidenced by the bilayers visible in the periphery in Fig. 10B and Fig. S27,† as well as the differential contrast as a function of position throughout the structures. Furthermore, there does not appear to be a significant change in the morphology after irradiation, although a similar relative size decrease is observed, consistent with that depicted in Fig. 9.

Conclusions

A novel monomer, nitrobenzyl hydroxypropyl methacrylate, was incorporated into amphiphilic block copolymers to afford UV-responsive polymeric assemblies. Nb 94 assembled into vesicles with an $R_{\rm h}$ of 235 nm and transitioned to spherical micelles with an $R_{\rm h}$ of 27 nm after 21 min of UV irradiation. At intermediate irradiation times, the structures initially increased in radius, forming aggregates which appeared to be transient structures from which micelles began to bud off. Depolarized DLS did not show evidence of wormlike micelles as an intermediate structure, supporting the proposed budding mechanism. Assemblies of Nb 176 appeared to be large compound vesicles with an $R_{\rm h}$ of 973 nm, which decreased to roughly 700 nm after ca. 5 hours of UV-irradiation. Unlike Nb 94 assemblies, Nb 176 assemblies did

not appear to undergo a morphological transition, likely due to its longer hydrophobic block.

This study is one of the few examples of a light-induced morphology change based on a change in the hydrophobic/hydrophilic balance of the polymer. Key insight was gained about the kinetics and intermediate structures of the morphology transition, deepening our understanding of morphological transitions of self-assembled polymeric structures.

Conflicts of interest

There are no conflicts to declare.

Acknowledgements

Authors thank other members of the Savin and Sumerlin groups for helpful discussion. Resources provided by the University of Florida Mass Spectrometry Research and Education Center were funded by NIH S10 OD021758-01A1. This project was funded in part by NSF CHE-1539347 (DAS) and NSF DMR-1904631 (BSS).

Notes and references

- 1 S. Jain and F. S. Bates, *Macromolecules*, 2004, 37, 1511–1523.
- 2 E. B. Zhulina, M. Adam, I. Larue, S. S. Sheiko and M. Rubinstein, *Macromolecules*, 2005, 38, 5330–5351.
- 3 C. Giacomelli, V. Schmidt, K. Aissou and R. Borsali, *Langmuir*, 2010, **26**, 15734–15744.
- 4 Y. Mai and A. Eisenberg, Chem. Soc. Rev., 2012, 41, 5969.
- N. J. Warren, O. O. Mykhaylyk, D. Mahmood, A. J. Ryan and S. P. Armes, *J. Am. Chem. Soc.*, 2014, 136, 1023–1033.
- 6 J. Du, Y. Tang, A. L. Lewis and S. P. Armes, *J. Am. Chem. Soc.*, 2005, **127**, 17982–17983.
- 7 D. Huang, Y. Zhuang, H. Shen, F. Yang, X. Wang and D. Wu, *Mater. Sci. Eng.*, C, 2018, 82, 60–68.
- 8 H. Gaballa, S. Lin, J. Shang, S. Meier and P. Theato, *Polym. Chem.*, 2018, **9**, 3355–3358.
- 9 J. G. Ray, J. T. Ly and D. A. Savin, *Polym. Chem.*, 2011, 2, 1536.
- 10 J. G. Ray, S. S. Naik, E. A. Hoff, A. J. Johnson, J. T. Ly, C. P. Easterling, D. L. Patton and D. A. Savin, *Macromol. Rapid Commun.*, 2012, 33, 819–826.
- 11 C. J. Mable, L. A. Fielding, M. J. Derry, O. O. Mykhaylyk, P. Chambon and S. P. Armes, *Chem. Sci.*, 2018, 9, 1454– 1463.
- 12 K. E. Gebhardt, S. Ahn, G. Venkatachalam and D. A. Savin, *Langmuir*, 2007, 23, 2851–2856.
- 13 A. P. Bapat, J. G. Ray, D. A. Savin, E. A. Hoff, D. L. Patton and B. S. Sumerlin, *Polym. Chem.*, 2012, 3, 3112–3120.
- 14 E. G. Wilborn, C. M. Gregory, C. A. Machado, T. M. Page, W. Ramos, M. A. Hunter, K. M. Smith, S. E. Gosting,

- R. Tran, K. L. Varney, D. A. Savin and P. J. Costanzo, *Macromolecules*, 2019, **52**, 1308–1316.
- 15 S. S. Naik, J. G. Ray and D. A. Savin, *Langmuir*, 2011, 27, 7231–7240.
- 16 C. A. Figg, A. Simula, A. G. Kalkidan, B. S. Tucker, D. M. Haddleton and B. S. Sumerlin, *Chem. Sci.*, 2015, 6, 1230–1236.
- 17 F. Sun, Y. Wang, Y. Wei, G. Cheng and G. Ma, J. Bioact. Compat. Polym., 2014, 29, 301–317.
- 18 N. P. Truong, M. R. Whittaker, A. Anastasaki, D. M. Haddleton, J. F. Quinn and T. P. Davis, *Polym. Chem.*, 2016, 7, 430–440.
- 19 L. He, S. Vibhagool, H. Zhao, V. Hoven and P. Theato, *Macromol. Chem. Phys.*, 2018, **1800104**, 1–5.
- 20 Y. Cai, K. B. Aubrecht and R. B. Grubbs, J. Am. Chem. Soc., 2010, 133, 1058–1065.
- 21 H. Lee, W. Wu, J. K. Oh, L. Mueller, G. Sherwood, L. Peteanu, T. Kowalewski and K. Matyjaszewski, *Angew. Chem.*, 2007, 46, 2453–2457.
- 22 S. J. Lim, C. J. Carling, C. C. Warford, D. Hsiao, B. D. Gates and N. R. Branda, *Dyes Pigm*, 2011, 89, 230–235.
- 23 A. P. Goodwin, J. L. Mynar, Y. Ma, G. R. Fleming and J. M. J. Fréchet, J. Am. Chem. Soc., 2005, 127, 9952–9953.
- 24 L. Sun, Y. Yang, C. M. Dong and Y. Wei, *Small*, 2011, 7, 401–406.
- 25 G. Y. Liu, C. J. Chen, D. D. Li, S. S. Wang and J. Ji, *J. Mater. Chem.*, 2012, 22, 16865–16871.
- 26 J. He, X. Tong and Y. Zhao, *Macromolecules*, 2009, 42, 4845–4852.
- 27 M. Klinger, L. P. Tolbod, K. V. Gothelf and P. R. Ogilby, ACS Appl. Mater. Interfaces, 2009, 1, 661–667.
- 28 A. Guo, G. Liu and J. Tao, *Macromolecules*, 1996, **29**, 2487–2493.
- 29 C. Nam, Y. Qin, Y. S. Park, H. Hlaing, X. Lu, B. M. Ocko, C. T. Black and R. B. Grubbs, *Macromolecules*, 2012, 45, 2338–2347.
- 30 S. Kumar, J. F. Allard, D. Morris, Y. L. Dory, M. Lepage and Y. Zhao, *J. Mater. Chem.*, 2012, 22, 7252–7257.
- 31 J. Jiang, X. Tong and Y. Zhao, *J. Am. Chem. Soc.*, 2005, **127**, 8290–8291.
- 32 J. W. Woodcock, R. A. E. Wright, X. Jiang, T. G. O'Lenick and B. Zhao, *Soft Matter*, 2010, **6**, 3325–3336.
- 33 S. Lin, X. Huang, R. Guo, S. Chen, J. Lan and P. Theato, *J. Polym. Sci., Part A: Polym. Chem.*, 2019, **57**, 1580–1586.
- 34 G. Wang, X. Tong and Y. Zhao, *Macromolecules*, 2004, 37, 8911–8917.
- 35 J. Jiang, B. Qi, M. Lepage and Y. Zhao, *Macromolecules*, 2007, **40**, 790–792.
- 36 E. Cabane, V. Malinova and W. Meier, *Macromol. Chem. Phys.*, 2010, 211, 1847–1856.
- 37 D. Han, X. Tong and Y. Zhao, *Macromolecules*, 2011, 44, 437-439.
- 38 J. Jiang, X. Tong, D. Morris and Y. Zhao, *Macromolecules*, 2006, **39**, 4633–4640.
- 39 G. Liu, L. Zhou, Y. Guan, Y. Su and C. Dong, *Macromol. Rapid Commun.*, 2014, 35, 1673–1678.

- 40 Y. Mitsukami, M. S. Donovan, A. B. Lowe and C. L. McCormick, *Macromolecules*, 2001, 34, 2248–2256.
- 41 A. Blanazs, A. J. Ryan and S. P. Armes, *Macromolecules*, 2012, 45, 5099–5107.
- 42 C. A. Figg, R. N. Carmean, K. C. Bentz, S. Mukherjee, D. A. Savin and B. S. Sumerlin, *Macromolecules*, 2017, **50**, 935–943.
- 43 J.-M. Schumers, C.-A. Fustin, A. Can, R. Hoogenboom, U. S. Schubert and J.-F. Gohy, *J. Polym. Sci., Part A: Polym. Chem.*, 2009, 47, 6504–6513.
- 44 Y. Yu, L. Zhang and A. Eisenberg, *Macromolecules*, 1998, **31**, 1144–1154.
- 45 P. C. Hiemenz and T. P. Lodge, *Polymer Chemistry*, CRC Press, Boca Raton, FL, 2nd edn, 2007.
- 46 A. Blanazs, J. Madsen, G. Battaglia, A. J. Ryan and S. P. Armes, *J. Am. Chem. Soc.*, 2011, 133, 16581–16587.
- 47 R. Pecora, *Dynamic Light Scattering*, Springer Science & Business Media, 1985.
- 48 F. Ahmed, R. I. Pakunlu, A. Brannan, F. Bates, T. Minko and D. E. Discher, *J. Controlled Release*, 2006, **116**, 150–158.